Pure appl. geophys. 166 (2009) 301–324
0033–4553/09/010301–24
DOI 10.1007/s00024-008-0437-2

Pure and Applied Geophysics

Analysis of Observed and Predicted Tsunami Travel Times for the Pacific and Indian Oceans

PAUL WESSEL

Abstract—I have examined over 1500 historical tsunami travel-time records for 127 tsunamigenic earthquakes that occurred in the Pacific and Indian Oceans. After subjecting the observations to simple tests to rule out gross errors I compare the remaining reports to simple travel-time predictions using Huygens method and the long-wave approximation, thus simulating the calculations that typically take place in a tsunami warning situation. In general, I find a high correspondence between predicted and reported travel times however, significant departures exist. Some outliers imply significantly slower propagation speeds than predicted; many of these are clearly the consequences of observers not being able to detect the (possibly weak?) first arrivals. Other outliers imply excessively long predicted travel times. These outliers reflect peculiar geometric and bathymetric conditions that are poorly represented in global bathymetric grids, leading to longer propagation paths and consequently increased travel times. Analysis of Δt, the difference between observed and predicted travel time, yields a mean Δt of 19 minutes with a standard deviation of 131 minutes. Robust statistics, being less sensitive to outliers, yield a median Δt of just 18 seconds and a median absolute deviation of 33 minutes. Care is needed to process bathymetry to avoid excessive travel-time delays in shallow areas. I also show that a 2×2 arc minute grid yields better results that a 5×5 arc minute grid; the latter in general yielding slightly slower propagation predictions. The largest remaining source of error appears to be the inadequacy of the point-source approximation to the finite tsunami-generating area.

Key words: Tsunami travel-time prediction, statistics, bathymetry.

1. *Introduction*

Historically, the Pacific has experienced several basin-wide tsunamis following large tsunamigenic earthquakes from various areas of the subducting plate boundary (e.g., DUDLEY, 1998). Of particular importance is the April 1, 1946 Aleutian earthquake whose powerful tsunami led to widespread destruction and numerous deaths (e.g., SHEPARD *et al.*, 1950); it also gave birth to the early U.S. tsunami warning system. In contrast, tsunamigenic earthquakes in other oceans have been much less frequent and thus warning centers were generally lacking; the calamitous 2004 Sumatra tsunami has now ushered in a new era in tsunami detection and preparedness. Designed to monitor their regions for potentially destructive tsunamis, warning centers, such as the U.S. Pacific and Alaska

---

Department of Geology and Geophysics, School of Ocean and Earth Sciences and Technology, University of Hawaii at Manoa, 1680 East-West Rd. Honolulu, HI 96822, U.S.A. E-mail: pwessel@hawaii.edu

tsunami warning centers, must routinely evaluate predicted tsunami travel times from the epicenters of potentially tsunamigenic earthquakes. Typically, it is not known until tide gauge or tsunameter data become available whether or not a particular large earthquake has generated an ocean-wide tsunami. In the mean time, the authorities may calculate travel times to a large number of tide stations and warning points in the Pacific. These estimated times of arrival (ETA) are incorporated into various communications from the warning agencies to local, state, and international civil defense agencies so that first responders will have an accurate estimate of when the first wave is likely to arrive. Because the premium is on responding quickly in a possible emergency situation, many warning agencies employ a rapid first-arrival methodology where no dynamic calculation of the waves is performed; i.e., no prediction of wave amplitude is attempted. Such dynamic calculations require detailed knowledge of the source, are usually done after an event, and may require considerable computational power (e.g., KOWALIK *et al.*, 2005). Simple estimates can be obtained by using the long-wave approximation (e.g., MADER, 2004; MEI, 1989), i.e., it is assumed that the tsunami will propagate away from the epicenter at a velocity given by

$$v(\vec{x}) = \sqrt{g(\vec{x})z(\vec{x})}, \tag{1}$$

where g is the vertical gravitational attraction, z is the local water depth, and $\vec{x}$ is the position vector. The program TTT from Geoware (GEOWARE, 2007) calculates these velocities based on an input bathymetry grid and uses Huygens' constructions to propagate the wave front from the epicenter to all nodes on the grid.

There are several situations in which these predicted ETAs may not match observed arrival times of the tsunami waves, including but not limited to the following:

1. The bathymetry grid is not accurate.
2. The epicenter is not well located, or the origin time is uncertain.
3. The epicenter is on land and a pseudo-epicenter off the coast must be selected.
4. The point approximation to the epicenter inadequately represents the rupture zone.
5. Nonlinear propagation effects may be important in shallow water.
6. The observed travel times represent later arrivals.

It is therefore of interest to examine historical tsunamigenic events in the Pacific and Indian Oceans and compare observed travel times to predictions made with the methodology currently in place at many warning centers. Given such data one may derive statistical information about the accuracy of these rapidly calculated ETAs. In particular, I wish to examine the statistical properties of Δt, the discrepancy between observed and predicted travel times, and determine if there are significant systematic variations in Δt. For instance, given that earthquakes with epicenters on land can excite tsunamis, how does Δt vary with location of the pseudo-epicenter location chosen for such earthquakes? Finally, I will examine to what degree the various error sources listed above are responsible for large Δt and what can be done to ensure the most accurate predictions in an emergency situation.

2. *Methodology*

I have examined the NGDC database of tsunamigenic earthquakes and associated observed first arrival tsunami travel times to numerous stations (National Geophysical Data Center, 2007). From this database 127 tsunamigenic earthquakes were identified as having produced observable tsunamis with well-determined origin times and locations. In selecting this subset I examined definite tsunamis since 1800 with runup reports, an earthquake magnitude of 6 or above, and an epicenter in the Pacific or Indian Oceans (Fig. 1); the overwhelming majority of events are from the Pacific basin. Travel-time calculations relied on the global 2×2 arc minute bathymetry grid ETOPO2 (National Geophysical Data Center, 2006) which itself derives most of its oceanic depths from the predicted/calibrated bathymetry based on satellite altimetry and shipboard bathymetry (Smith and Sandwell, 1994; 1997). To prevent excessive travel time overestimates in cases when the earthquake occurred beneath very shallow water (or for epicenters on land) I relocated the epicenter to the nearest node with a depth of

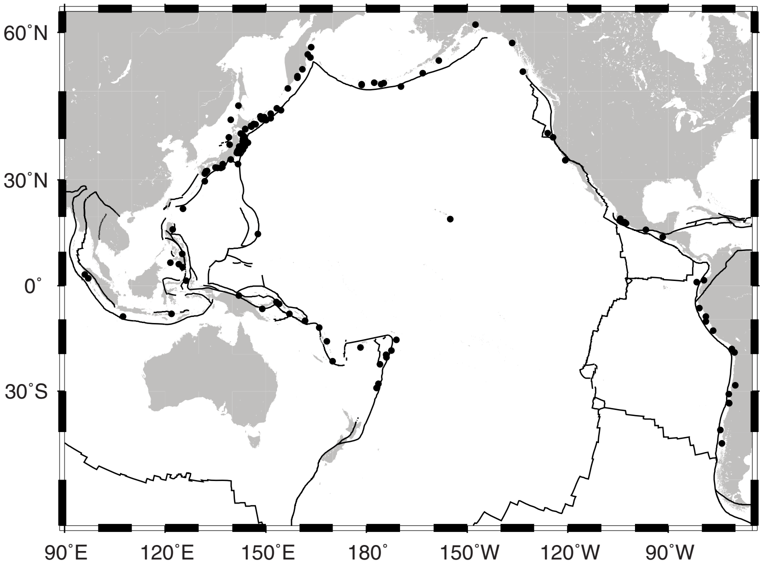

Figure 1
Location of 127 earthquakes identified as tsunamigenic events in the NOAA database. For each event I computed a global 2’×2’ travel-time grid and sampled the travel times at all stations that reported an observed travel time, yielding over 1500 pairs of reported and predicted travel times.

at least 25 m. For consistency, and to examine far-field propagation of the most devastating tsunamis, global 2×2 arc minute travel-time grids were generated for each of the 127 events considered, even though only a few are known to have propagated beyond the Pacific (or Indian) basins. For warning center operations, typically only a regional (e.g., Pacific-wide or Indian-wide) calculation is required; at 2×2 arc minute resolution a Pacific-wide ETA grid is obtained within 1–2 minutes on a fast workstation; a slightly cruder 5×5 arc minute solution takes less than 10 seconds. Because most warning operations will automatically determine the epicenter and magnitude of an earthquake (or obtain this information from other agencies), the tsunami travel-time calculations may be launched automatically for earthquakes over a certain magnitude threshold and the resulting travel-time grid will be ready for analysis almost immediately. The output travel-time grids are compatible with the Generic Mapping Tools (e.g., WESSEL and SMITH, 1998), which were used extensively in this analysis, and are available upon request.

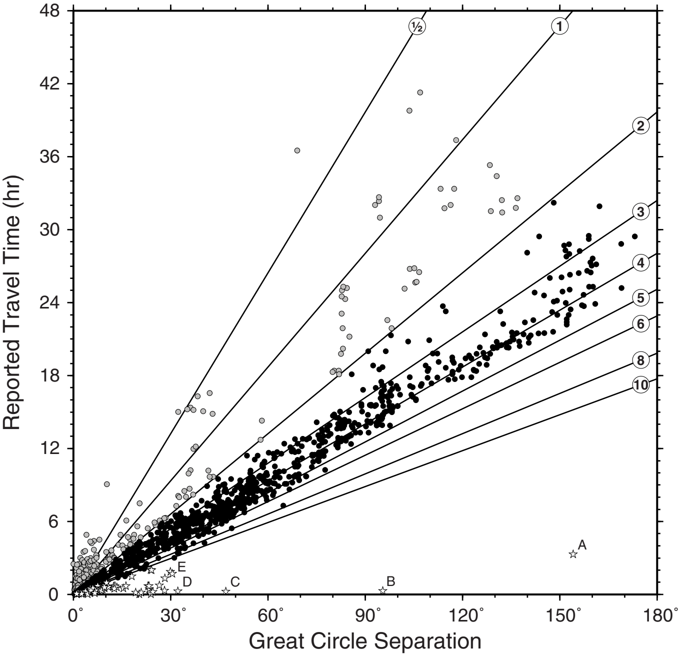

Figure 2

Reported travel times for the 127 earthquakes considered in the study, plotted versus the great circle distance between epicenter and recording station. Straight lines show travel times predicted by Eq. (1) for various average water depths (see labels, in km). Reported travel times above the 2 km-depth prediction (gray circles) are possibly late arrivals whereas times below the 11 km depth prediction may largely reflect erroneous tabulations (open stars), especially for the longer distances.

3. Analysis

3.1. Consistency of Reported Tsunami Travel Times

Prior to analyzing predictions I examined reported travel times versus the great circle separation between epicenter and reporting station; this distance represents the minimum path length traveled by any tsunami wave. Given Eq. (1) one can predict this relationship for a constant water depth. Figure 2 reveals several outliers that clearly indicate problems with the reported data. For instance, several reported travel times are much too short given the minimum distance the waves must have traveled. The outlier labeled "A" is the reported travel time from a 1922 earthquake in northern Chile to Aburatsubo, Japan. The distance is thus correct but one would expect a travel time closer to one day instead of the reported 198 minutes (3.3 hours). Perhaps the observed travel time originally was 19.8 hours (which is still too fast) but somehow ended up in the NOAA archive as 198 minutes. Outlier "B" from 2006 is more humorous, as the reasonable travel time from an Indonesian tsunami to Christmas Island (Indian Ocean) became associated with the other Christmas Island located in the Pacific, thus being archived with wrong metadata. Outlier C is simply a seiche registered in Freeport, Texas that was excited by the seismic tremors of the momentous 1964 Good Friday earthquake; thus, the travel time does not represent a typical tsunami phenomenon. Outlier D reflects another clerical error where the travel time from a 2006 earthquake in the Kuril Islands reportedly only took 16 minutes to reach the Shumagin Islands, Alaska over 3500 km to the west. Finally, outlier E is another Japanese recording (from Tsurushima) following a 1923 earthquake in Kamchatka. Again, I suspect the reported 10.2 minutes might originally have been 10.2 hours, and that many of the remaining outliers are likely to have similarly trivial explanations.

These data are further analyzed in Figure 3, which displays the equivalent average water depths, z_{ave}, required to reconcile reported travel times and their minimum distance of travel (via Eq. 1). All in all, 61 reports gave z_{ave} exceeding 11,022 m, which is the oceans' largest observed depth. These 61 are clearly all outliers and will be excluded from further consideration. Obviously, many others with slightly smaller z_{ave} are likely to be outliers as well but I have no clear cut-off criteria to apply and the distribution appears fairly continuous (see Fig. 3). Figure 2 also shows (as gray circles) reported travel times that appear too slow (equivalent average depth < 2 km). Certainly, for the more distant events these excessive travel times most likely reflect later arrivals, implying the first wave simply was too small to be noticed. Figure 3 suggests a possible hachured region where observations most likely come from later arrivals; again, no clear-cut criterion is available to separate these from first-wave arrivals and I will retain the remaining 1476 data pairs in the subsequent analysis.

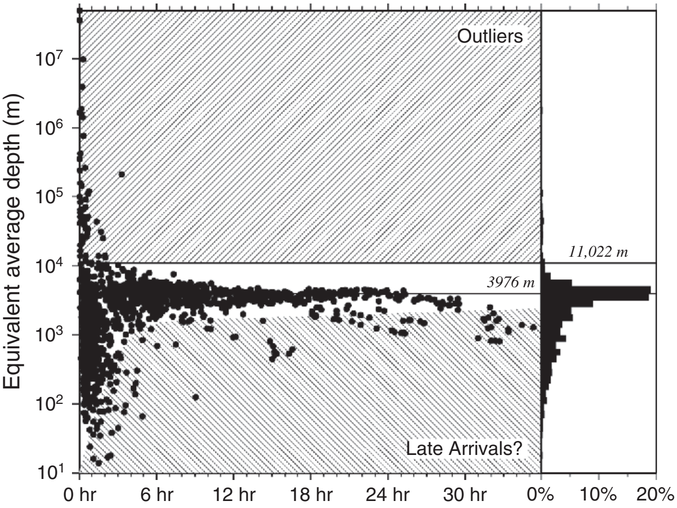

Figure 3
Equivalent average water depth (z_{ave}) versus reported travel times for data points in Figure 2. Most reported values are compatible with the Pacific mean ocean floor depth (3976 m). A total of 61 observations have a z_{ave} that exceeds the largest depth on Earth (11,022 m); these are considered clear outliers and are most likely clerical errors. Many values correspond to very shallow depths, probably reflecting overestimates of actual travel times (e.g., the detection of later rather than first arrivals). The lower hachured regions suggest an envelope for such later arrivals.

3.2. Simply Predicted Tsunami Travel Times

For each of the 127 events I calculated predicted travel-times on a global 2×2 minute grid, from which I made a detailed travel-time contour map, showing not only the (global) travel-time predictions but displaying the locations of stations from which reported travel times are available. These maps also include a simple graph of predicted versus observed travel time for these stations, and summarize the differences, Δt, between these pairs of values in standard box-and-whisker diagrams. In this paper I will only highlight some of these events individually; high-resolution PDF versions of all 127 event maps are available from the author's website (http://www.soest.hawaii.edu/pwessel/ttt). Figure 4 shows the results for the propagation of the tsunami wave front following the large 1960 Chile earthquake; here limited to the Pacific region only. The travel times are color-coded, with shading reflecting the shape of the underlying bathymetry. Over 100 tide stations, all in the Pacific, registered the arrival of this tsunami that took numerous lives, particularly in Hawaii and Japan, in addition to the local devastation in Chile (e.g., DUDLEY, 1998). None of the reported values have equivalent average depths exceeding 11,022 m. A direct comparison of observed and predicted travel times gives a correlation of 0.98, with a median Δt of only 14 minutes. However, note the several outlying points in the travel-time graph (Fig. 5). A closer inspection

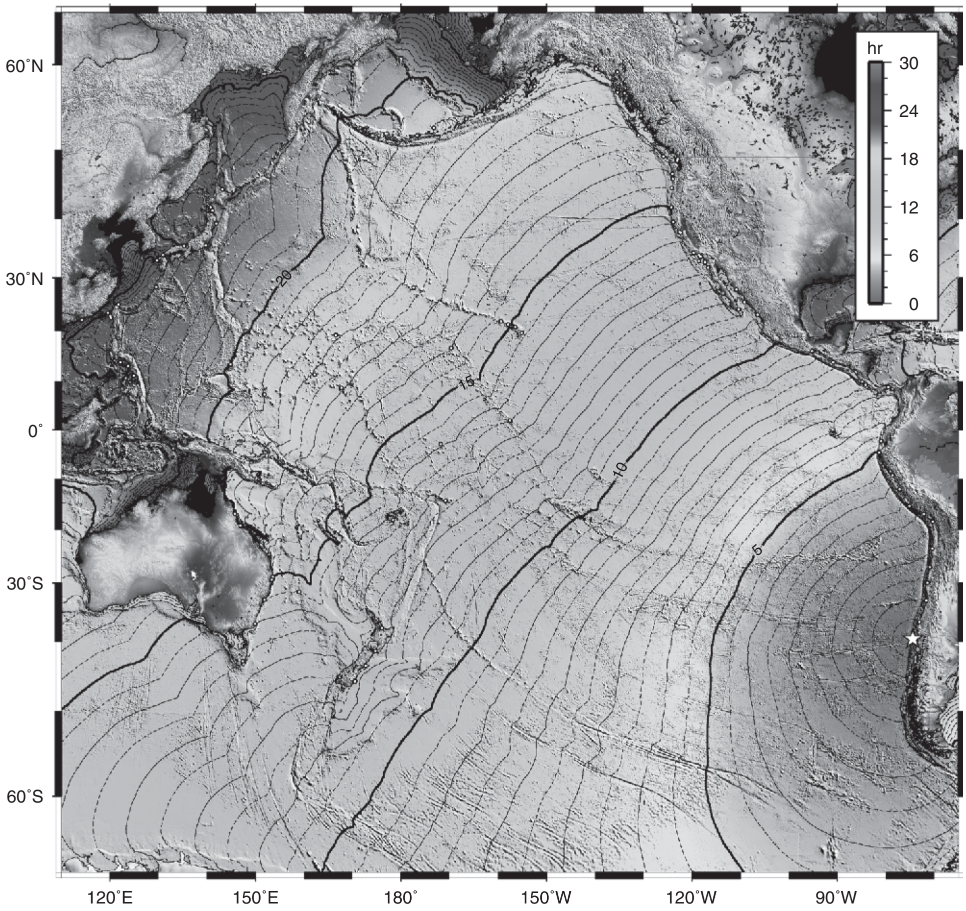

Figure 4
Predicted travel times for the Pacific-wide tsunami produced by the large 1960 Chile earthquake. Star indicates the point-source epicenter used for the calculation, with the 104 stations that reported travel times shown as white circles. Shading of travel times is provided by the bathymetry. Solid contours are hourly with 30-minute dashed contours in between.

shows that the single point for which the prediction exceeds the observed by several hours represents Punta Arenas in the far south of Chile. Given its sheltered position in the Strait of Magellan behind the Chilean Archipelago, the predicted travel time has been overestimated; it is likely that in this situation the simplicity of Eq. (1) poorly approximates the physics of wave propagation. Fortunately, the same island obstructions that lead to the excess in predicted travel time are also likely to attenuate truly dangerous waves before they arrive in Punta Arenas.

While the 1:1 correlation line is a remarkably good lower bound for all remaining observed travel times, there are several observations that are many hours slower than the

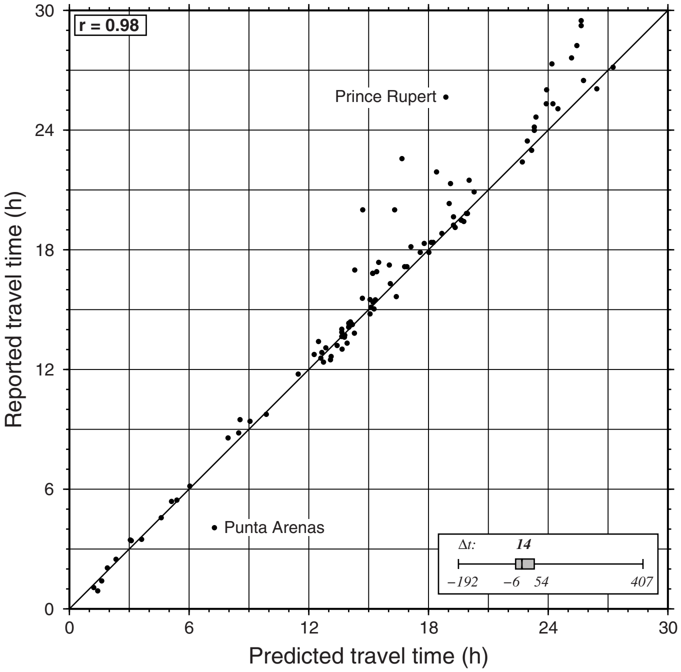

Figure 5
Reported versus predicted tsunami travel times for all 104 stations that observed the 1960 Chile tsunami. The 1:1 line represents perfect correlation. Large departures from this trend appear to be caused by excessive predicted travel times in shallow, narrow fiords (e.g., Punta Arenas, −3 hours) or a failure to detect the first arrivals (e.g., Prince Rupert, +6 hours). The box-and-whisker diagram summarizes the statistics of Δt; the differences between reported and predicted travel time (in minutes). The median Δt is +14 minutes.

corresponding predictions. Examining these points reveals that the slower observations for predictions in the 14–20 hour range are mostly associated with stations on the U.S. and Canadian west coast, many of which are sheltered in narrow inlets and sounds. Similarly, the slow arrivals after the first full day of propagation are mostly stations on the west-facing sides of Japan, Taiwan, and the Philippines. It would seem that these outliers represent later arrivals in locations where the first wave was not particularly energetic.

3.3. Statistical Analysis of Travel Times

Figure 6 shows all observed tsunami travel times plotted against the corresponding predicted travel times; the 61 points with excessive z_{ave} have been excluded. Again, if travel-time observations and predictions both faithfully reflected reality then all points should fall on a straight line with slope 1:1; clearly, this is not the case. However, as in the case of the 1960 event we do find a strong tendency for points to cluster around this line, however there is significant scatter, some systematic offsets, and some large outliers. A peculiar feature of this plot is the appearance of a secondary trend that parallels the main 1:1 line but shifted by almost three hours of excess predicted travel time. During the analysis it became clear that the 1964 Prince Williams Sound, Alaska earthquake posed a particular problem when comparing predictions to observed travel times. Even a casual inspection of the travel-time correlation chart (white circles in Fig. 6) reveals that the predicted travel times are all close to three hours too long. This consistency for all observations points to a problem originating in the area near the epicenter. Early studies have demonstrated, by backward propagation of travel times, that the tsunami source area had to be located further out on the continental shelf, far from the epicenter (e.g., HATORI, 1981; PARARAS-CARAYANIS, 1967). Figure 7a presents a Mercator map of the Gulf of Alaska and indicates the reported location of the epicenter (star). As reported, the epicenter falls on land (e.g., SHERBURNE *et al.*, 1969) and therefore was relocated to the nearest ocean node of at least 25 m depth. The bathymetry in and near the area is

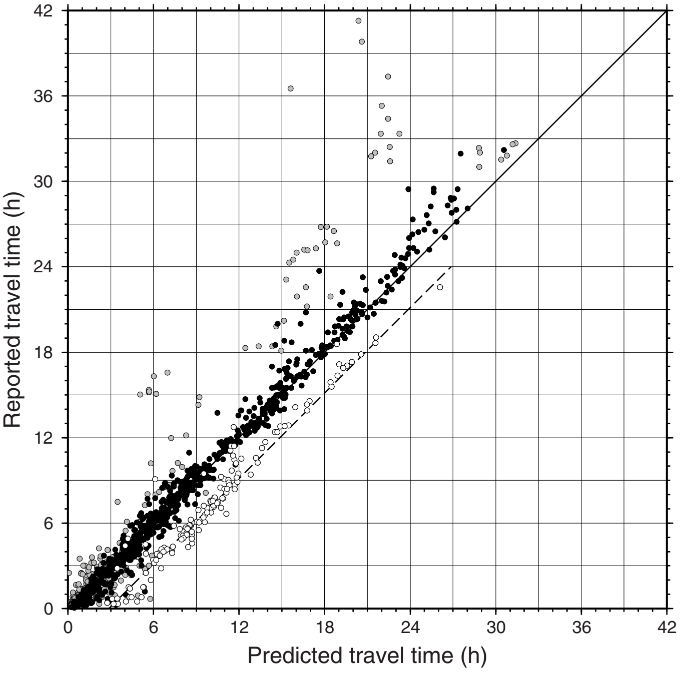

Figure 6
Correlation plot of all 1476 pairs of reported and predicted tsunami travel times. Color-coding as in Figure 2; outliers (stars) have been excluded. Other extreme outliers are noted, both above and below the trend line. The cluster of points (white) sub-parallel to the trend line ensues from reports of the great 1964 Prince Williams Sound earthquake in Alaska (see text).

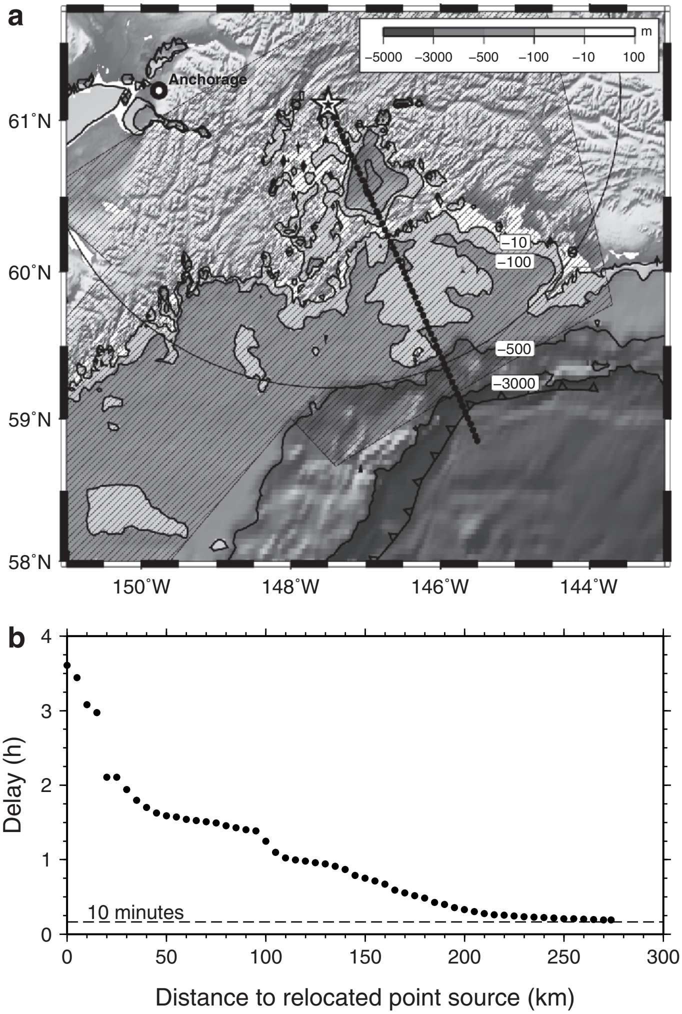

Figure 7

a) Coastlines and bathymetry near the site of the 1964 Alaska earthquake (star). Bathymetry shows extended shallow water depths on the continental margin. Hachured areas are uplifted blocks determined by joint geodetic and tsunami inversion by Johnson *et al.* (1996). Red dots indicate alternative point source locations for improved travel-time calculations, up to 275 km from the epicenter and toward the trench. **b**) Average delay (predicted minus reported tsunami travel time) obtained by using different point source locations. The major delays are caused by low propagation speed in shallow waters and the fact that the tsunami generation took place closer to the continental edge.

particularly shallow, which adds considerable propagation time to all stations. However, the main cause of the delays lies in the nature of the tsunami generation. Studies have shown that a large region of the continental shelf experienced significant crustal uplift in response to the earthquake (e.g., Christensen and Beck, 1994; Johnson *et al.*, 1996; Ruff

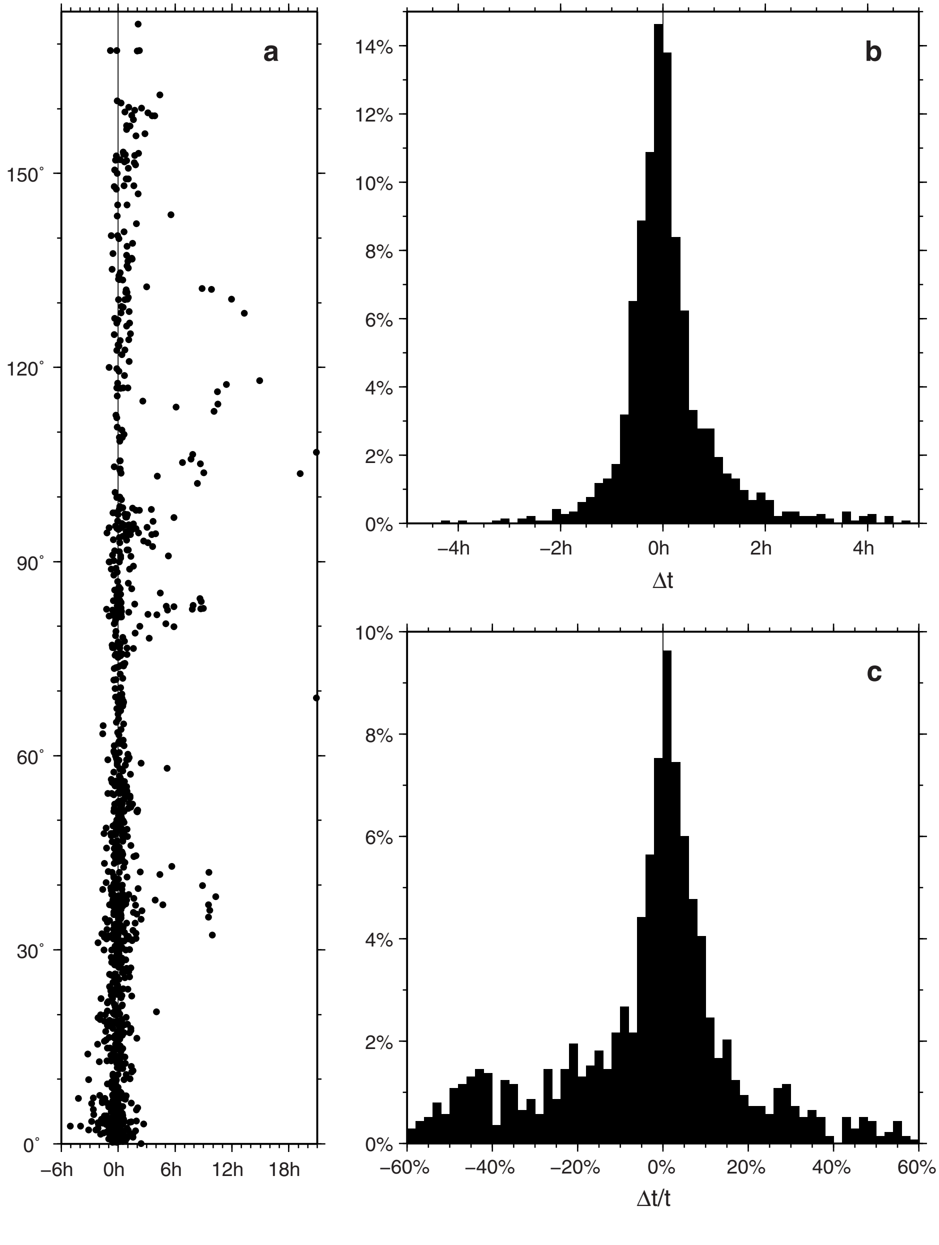

Figure 8

(a) Summary of Δt, the difference between reported and predicted tsunami travel times for all 1537 data pairs versus minimum travel distance (in degrees). (b) Histogram of Δt. The mean (median) value is 12 (-1.5) minutes with standard deviation (median absolute deviation) of 139 (35) minutes. Distribution has a longer tail to the right. (c) Same, but normalized by predicted travel time and reported in percent.

and KANAMORI, 1983), and it is this wide uplift of the water on the continental shelf that initiated the tsunami. In other words, a point source approximation turns out to be particularly poor for this event; however, this realization is in general not achieved until some time after the event.

To test this explanation I relocated the point source to increasingly more distant locations along a great circle from the epicenter to the nearest point on the trench

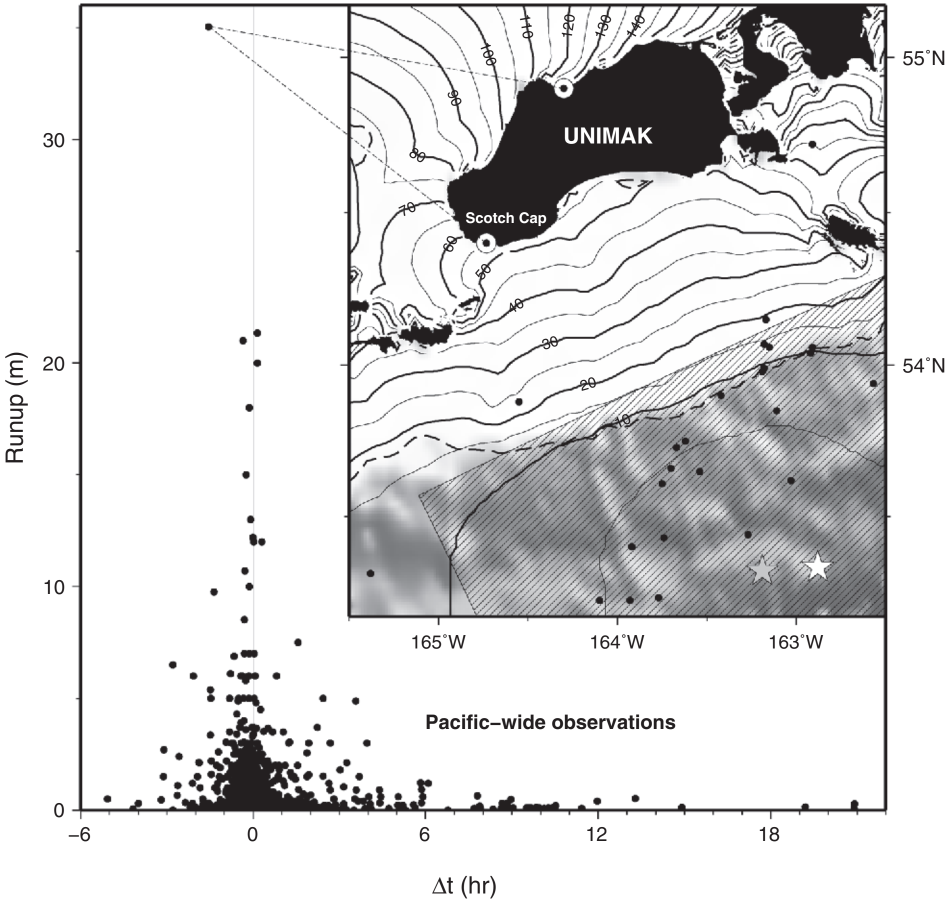

Figure 9

Distribution of tsunami runups (m) versus Δt. The larger runups have small Δt, suggesting larger Δt values may involve later arrivals. Note the large runup for the 1946 tsunami and its substantial travel-time prediction delay of ~1.5 hrs. Inset: Travel-time contours (in minutes) from epicenter (star) of 1946 Aleutian tsunami on shaded bathymetry. Gray star is epicenter reported in NOAA runup catalog. White star, solid circles, and hachured region are relocated epicenter, aftershocks, and best estimate of minimum rupture area, respectively (LOPEZ and OKAL, 2006). Dashed contour is 200-m isobath. The marked delay Δt for the largest runup reflects incorrect coordinates used for Scotch Cap (see text).

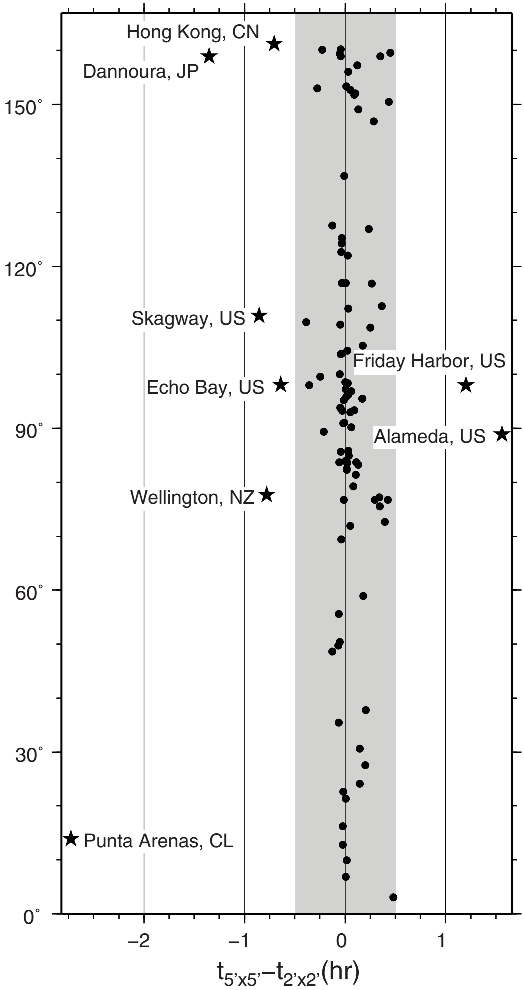

Figure 10
Sensitivity of predicted travel time due to bathymetry grid resolution. Differences in travel times (solid dots) calculated from 5×5 and 2×2 arc minute grids are shown at all stations reporting arrivals for the 1960 Chile event. I thoroughly investigated the causes of the largest discrepancies (named stations; solid stars) which all were related to geometry changes for shallow water pathways near the station (see text).

(Fig. 7a). I then ran the travel-time calculations on the 2×2 arc minute grid for the different point sources. The various travel-time delays were found by computing the mean Δt for each solution. Figure 7b shows the prediction delays versus the distance between reported epicenter and point source used. The delay is gradually reduced with distance and appears to approach asymptotically a ~10-minute level (for distances > 250 km). This distance corresponds to the outer boundary of the uplifted

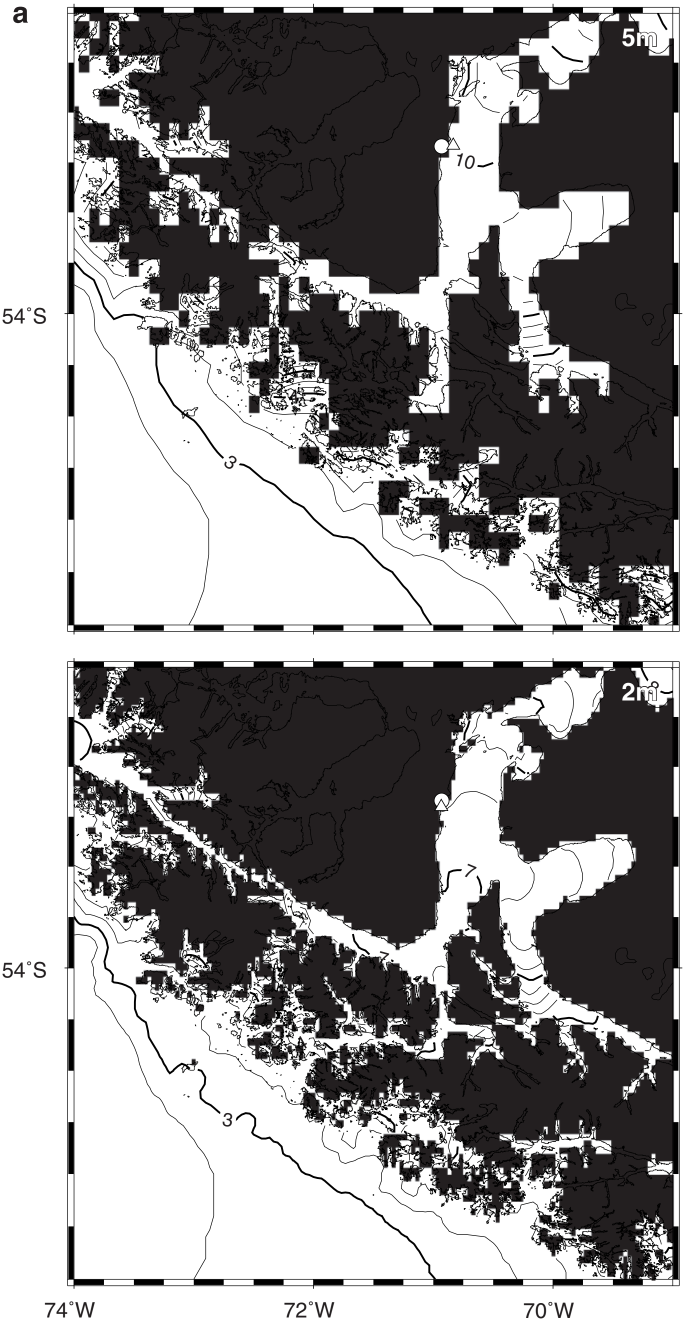
a
5m
10
3
54˚S
2m
7
3
54˚S
74˚W
72˚W
70˚W

◀ Figure 11

Comparison of bathymetry grid and predicted travel times for the 2×2 min (lower) and 5×5 min (upper) grids for the 1960 Chile event. Open circle is reported station location whereas open triangle is nearest node located in the water. (a) Punta Arenas, Chile, is located in the Strait of Magellan sheltered by the Chilean Archipelago. The different bathymetry resolutions result in different pathways and a shallower average depth. (b) Alameda, California, US in the San Francisco Bay. In the courser 5-min-grid the bay entrance is closed off, forcing the station to be relocated all the way to the Pacific coast and shortening the predicted time. (c) Dannoura, Japan is similar to Alameda, as the relocated station falls on the Japan Sea coast instead of in the Seto Inland Sea to the east of the artificial barrier blocking the Kanmon Strait.

blocks (hachured areas in Fig. 7a) determined from a joint inversion of geodetic data and tsunami waveforms (JOHNSON *et al.*, 1996). The remaining ~ 10 minute delay most likely reflects the non-point-source nature of the disturbance as well as other causes such as inaccurate bathymetry at reporting stations and inability to identify the arrival of the first wave.

Figure 8 presents a summary and histograms of Δt implied by the data in Figure 6 and augmented by the data for the 1964 tsunami after correcting for the inferred 2.92-hour bias. Figure 8a shows how $\Delta \mathrm{t}$ varies with epicenter-station separation. We clearly see late arrivals (positive Δt) increase for tsunami waves that traveled long distances, while prediction errors ($\Delta t < 0$) are most prevalent for stations not too distant from the tsunami nucleation area. Two different forms of analysis were pursued: (1) Figure 8b gives the standard histogram of the Δt distribution in terms of departures from the predicted value; (2) Figure 8c shows the same departure as a percentage relative to the predicted travel time. This approach was undertaken to show how the misfit varied with travel time. We note that the former quantity appears more normally distributed than the latter, nonetheless both have long tails, suggesting nonparametric statistics should be used to characterize the distributions. Whereas the mean and standard deviation of Δt are 19 and 131 minutes, respectively, the median and the median absolute deviation (MAD) are only -0.3 and 33 minutes, respectively. Clearly, the presence of late arrivals skews the mean away from the expected zero, which is well represented by the median. The percentages also are vulnerable to large scatter due to the normalization by small travel times; I find a median percentage of -0.2 and a MAD of 15%. These robust values represent typical uncertainties and exclude the few extreme cases.

3.4. *Runup and Predicted Travel Times*

One of many concerns for agencies responsible for issuing warnings is the possibility of overestimating travel times to some stations, such as would have been the case if the 1964 Alaska tsunami travel-time predictions were to be taken at face value. In comparing reported runups to both predicted and reported travel times I note: (1) The largest runups are associated with stations very close to the epicenter. For people in proximal regions of large earthquakes the best defense is to leave the coastal region and seek safety inland while there is still time. (2) Runups at stations with poor correlation between reported

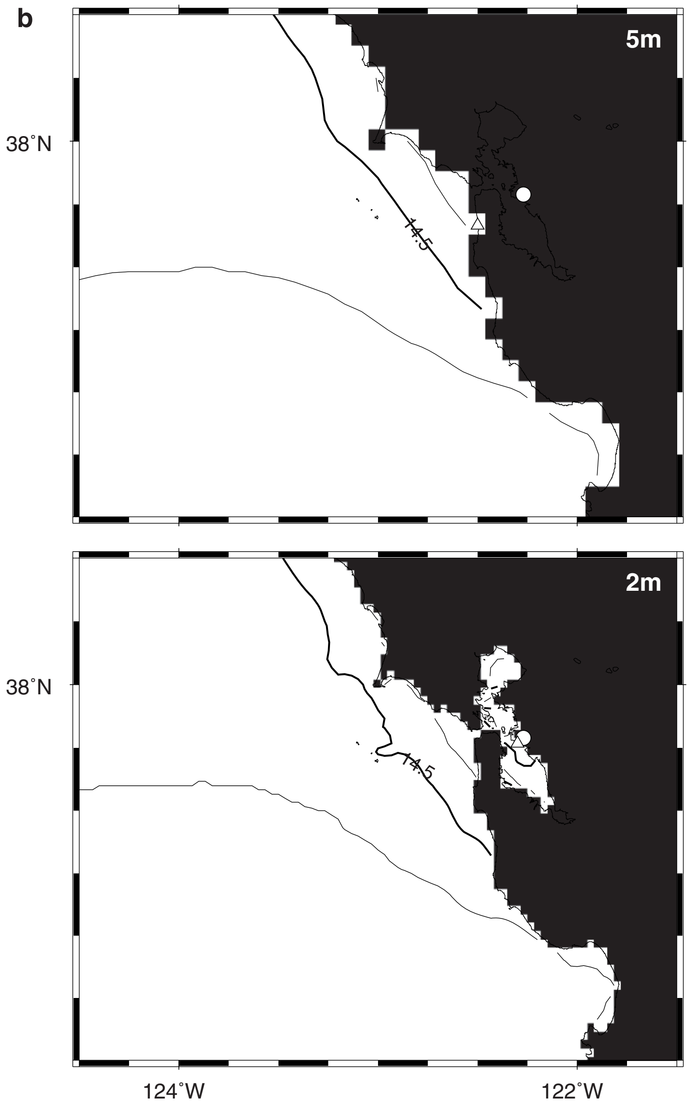

Figure 11
Contd.

and predicted travel times are insignificant. This is highlighted in Figure 9, which displays runups for all 1476 records; it is clear that, in general, the largest values have very small Δt. However, we note that the largest runup (> 35 m) has a disturbingly large prediction delay of 1.6 hours (as do some other runups in the 5–10 m range). This particular observation comes from Scotch Cap on Unimak Island, Alaska following the April 1, 1946 tsunami that originated on the slope to the south of Unimak Island. This

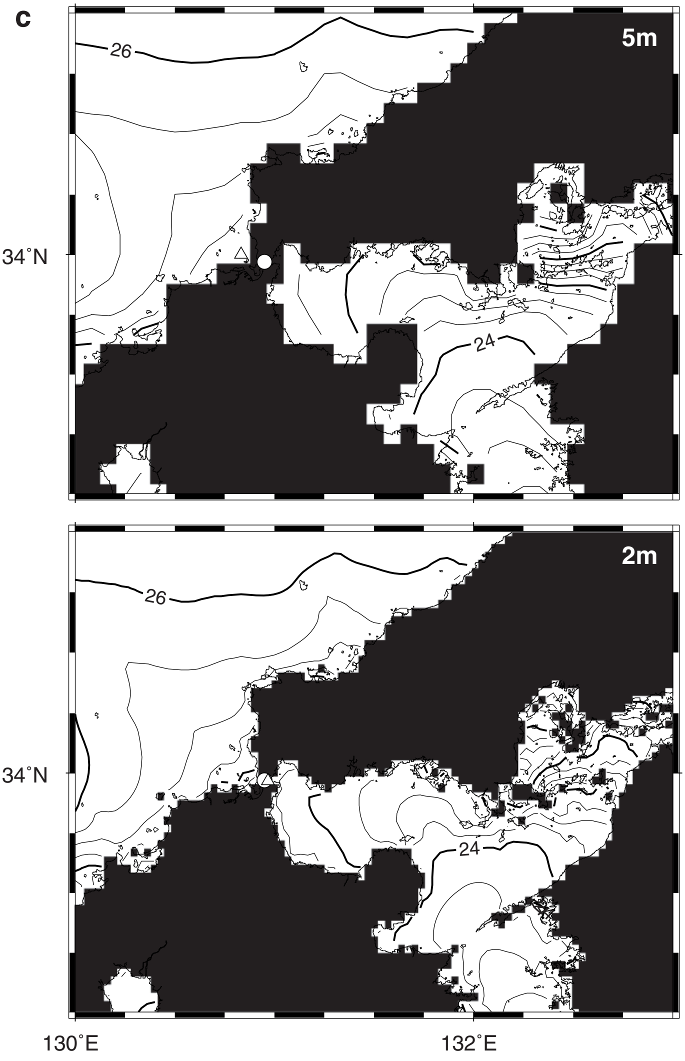

Figure 11
Contd.

tsunami is unusual in that it is generally assigned a relatively small magnitude (e.g., Pacheco and Sykes, 1992), yet its tsunami magnitude is 9.3 (Abe, 1979) and it produced very large runups focused in a narrow beam normal to the strike of the trench (Fryer *et al.*, 2004). A recent revision to the Scotch Cap runup even raises the value to 42 m (Okal *et al.*, 2003), and a reanalysis of long-period seismographs suggests the magnitude was probably closer to 8.5 (Lopez and Okal, 2006). Several studies have determined

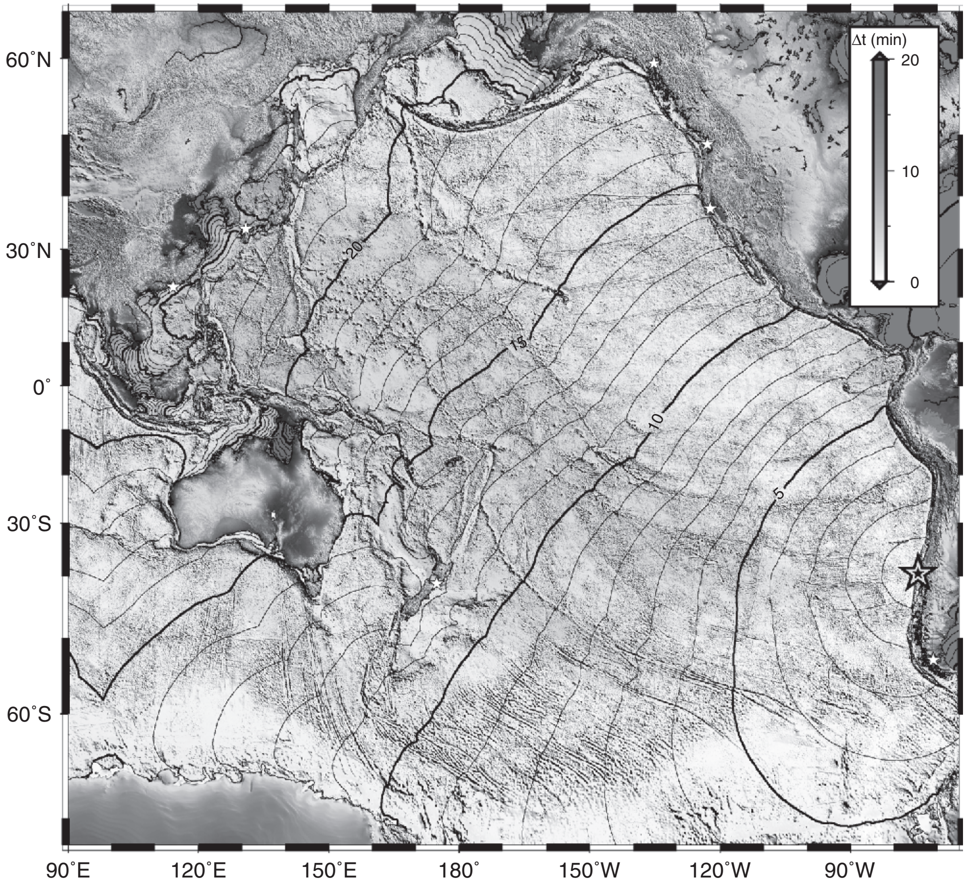

Figure 12
Color-coded differences between travel-time predictions for 2×2 and 5×5 arc minute bathymetry, with superimposed hourly travel-time- contours. Yellow star is epicenter location. The largest differences occur in shallow coastal areas such as between Australia/Papua New Guinea and the Yellow Sea between China and Korea. For > 97% of the Pacific nodes the difference in predicted travel time is less than 5 minutes. White stars denote locations of 8 outliers in Figure 10.

approximate fault plane solutions from the distribution of aftershocks (e.g., JOHNSON and SATAKE, 1997; LOPEZ and OKAL, 2006); hence the point source epicenter solution employed herein to obtain travel times may likely be inadequate in this case as well. However, from the map inset we can determine the main cause of the large Δ*t*: While the NOAA runup data base correctly reports the Scotch Cap observed travel time (48 minutes) and runup, it incorrectly lists as location the coordinates of a point on the north side of Unimak Island, near Cape Mordvinof. Using the Scotch Cap coordinates yields a revised predicted travel time of 53 minutes and an improved Δ*t* of only 5 minutes.

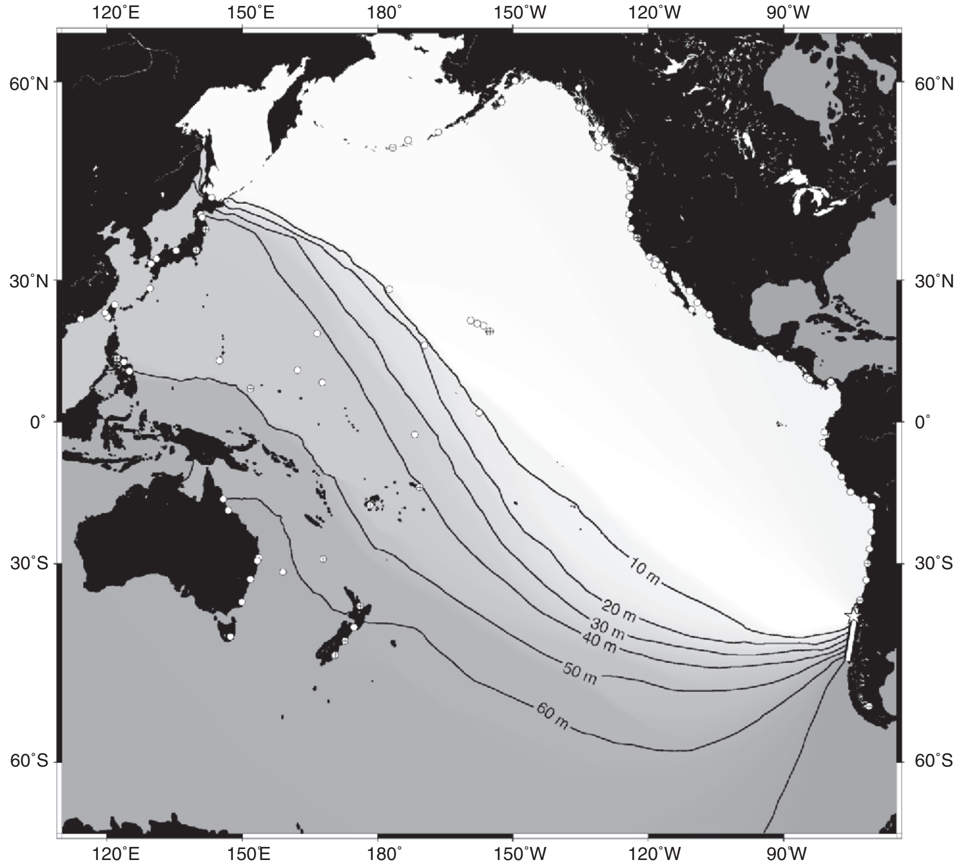

Figure 13
Differences in travel-time predictions for the 1960 Chile tsunami using a close approximation to the actual rupture area (white rectangle) versus the point-source epicenter solution (star). Contours (in minutes) project the effect being limited to the southern and western Pacific (shaded areas). Circles represent recording stations; crossed circles have predicted travel times that are slower than observed by 10 minutes or more.

3.5. *Effect of Using Coarser Bathymetry Grids*

Regardless of the method used to calculate travel times, any uncertainties in water depth will translate into uncertainties in the predictions. Equation (1) suggests uncertainties in depth are more critical for areas of shallow water where an underestimated depth can give rise to significant travel-time delays. One source of depth uncertainty comes from the preparation of gridded bathymetry. Given the 104 stations that reported observed travel times for the 1960 Chile tsunami, I repeated the travel-time calculation using a coarser, 5×5 arc minute global grid derived by filtering ETOPO2 with a 17-km median filter to avoid aliasing and to reduce the influence of narrow, shallow features in the derived grid. I then computed the difference in predicted travel-time to the 104 stations and plotted these differences versus the corresponding epicenter-to-station great circle distances (Fig. 10). While the differences have ~ zero mean we find a handful of significant outliers as well as a general variability with standard deviation of ~5 minutes. To determine the source of the larger outliers (stars) I thoroughly investigated each of the bathymetry grids near the eight named stations; here I discuss three representative examples that highlight the typical causes of such discrepancies. The remaining examples have similar albeit less severe characteristics.

Figure 11a shows travel-time grids for the 5×5 minute (upper) and 2×2 minute (lower) bathymetry grids. Black indicates nodes on land. The circle indicates the location of Punta Arenas in southern Chile where the two travel-time grids differ by almost 2 hours. Examination of the nodes quickly reveals differences between the two grid resolutions. While the finer 2×2 minute grid is able to preserve some of the narrow waterways between the numerous islands in the Chilean Archipelago and the Strait of Magellan, the 5×5 minute grid has closed off many of these pathways, resulting in two significantly different paths from epicenter to station. In this extreme case the 5×5 minute grid prediction would be almost 10 hours. Neither solutions come particularly close to the reported travel time of ~4 hours (7.3 vs. 10 hours).

Figure 11b shows the opposite situation occurring at the Alameda tide station inside San Francisco Bay, USA. Here, the narrow inlet (spanned by the Golden Gate Bridge) could not be represented in the coarser grid, resulting in the entire bay being land-locked. In such cases, the travel-time grid must be sampled at the ocean node nearest the tide station (triangle), which in this case is relocated to the Pacific coast. In comparison, the finer grid allows for propagation into the shallow bay, thus resulting in almost one hour longer travel time and a much better fit to the observed travel time.

Finally, Figure 11c displays the travel-time grids near the Japanese station Dannoura (circle). Again, the coarser grid is unable to represent the narrow Kanmon Strait connecting the Japan Sea to the Seto Inland Sea, and when the nearest node in the ocean is selected it falls on the western rather than eastern side of the artificial barrier. Hence, as the waves must propagate around Kyushu to reach the station, we find a delay of almost 2 hours relative to the 2×2-minute grid prediction. Interestingly, the reported travel time to Dannoura is 29.5 hours, which is about 4 hours longer than the 2×2-minute prediction. Based on Figure 2 it would appear that the reported arrival time corresponds to a later arrival; the bathymetry near the station is not as complicated as in the case of Punta Arenas, and hence the 4-hour difference is unlikely to reflect a prediction error.

By resampling the 5×5 minute travel time prediction grid onto a 2-minute grid we may compute the predicted differences for the entire Pacific (Fig. 12). It is noteworthy that the two grids differ by less than 5 minutes at ~97% of the grid nodes. The only significant deviations visible at this scale are differences in the 20–60 minute range for shallow areas between Australia and Papua New Guinea and in the Yellow Sea. The extreme cases in Figure 10 (white stars in Fig. 12) are not typical nodes in this regard, yet many tide stations are obviously located in shallow water near land and hence are affected locally by the grid resolution effect. We can also see a subtle delay effect due to the denser seamount populations in the Western Pacific. While the 5×5 minute predictions in general are slightly slower than the 2×2 minute predictions, a few areas show the opposite effect (e.g., off Alaska), again reflecting the difference in pathways when narrow waterways are not adequately represented in one of the grids.

4. Discussion

This investigation has found several characteristics of observed and predicted travel times and their statistical distribution and depth-dependency that may be of interest to both warning centers and tsunami researchers. However, given the simple approach used to predict travel times, the observations made in this study are more germane to the near-real-time response to a tsunami in progress when quick and accurate estimates of travel times are required. It is reassuring that the simple predictions based on Eq. (1) and the standard 2×2 minute bathymetric grid are quite consistent with reported travel times for the 127 tsunamis studied here (e.g., Fig. 6). However, there are clear departures from the expected 1:1 correlation and these have been examined in some detail. I have demonstrated that predictions in some cases have considerable delays and determined three main causes for these delays: (1) The inability of the epicenter point source to adequately represent the actual water impact that generated the tsunami, (2) occasional large changes in propagation geometry due to the finite spatial resolution of the global grids, and (3) uncertainties in depth for shallow water regions. Given Eq. (1), all significant bathymetric bias will occur in shallow waters. For any event, these areas are most likely to include the immediate regions surrounding both epicenter and observation points (or warning points). Warning agencies and tsunami researchers should therefore strive to acquire the best available local bathymetric data in all regions that fall in this category.

To exemplify the bias that may result from using a point source (i.e., the epicenter) for tsunami travel-time evaluation I contrast the predictions from the 1960 Chile tsunami using two different sources: (1) The reference calculation uses the reported epicenter (Fig. 4) which is what warning centers must use in a real-time warning situation, and (2) the rupture zone identified by PLAFKER and SAVAGE (1970). The latter source region extends over 1000 km southward from the epicenter and hence prediction of travel times south of the epicenter can be expected to differ. Figure 13 shows the difference in predicted travel time (in minutes) between the point- and line-source calculations. As anticipated the largest discrepancies are found to the south of a line from the epicenter to Japan, i.e., the shaded region. In particular, at stations in New Zealand and Australia the difference in predicted travel time is almost 1 hour. Stations that reported an observed travel time shorter than the reference prediction are shown with a crossed circle; the majority of such stations fall in the affected region. Of course, slow propagation in shallow waters near some stations and failure to detect first arrivals may have obscured the predicted trend to some extent.

In a warning situation the emphasis lies on preparing as accurate estimated times of arrival as possible. It is therefore of great concern that certain combinations of epicenter locations and station placements, when used with Eq. (1) and standard global bathymetric grids, yield travel times that are unacceptably delayed. Should such delayed predictions be presented as accurate they may cause considerable damage directly (by giving wrong information) and indirectly (by reducing the confidence the community has in warning centers). However, large tsunamigenic earthquakes do not occur daily, hence there is ample time between events to lay the groundwork required to avoid such overestimates. Given the rapidity with which travel-time estimates can be obtained, warning centers may explore the effects that epicenter and station location and bathymetry grid quality have on the predicted values. For instance, the finite number of tide stations and warning points could be explored in detail (such as was done in Fig. 11) to determine if the coordinates of the station should be adjusted to avoid particularly shallow areas and if important, but narrow water ways are well represented in the grid. Special processing of the bathymetry may be required to reduce delays and optimize travel-time predictions. Similarly, precalculations of tsunamis from anywhere along the ring of fire could be examined and used to identify regions where point source solutions may be particularly susceptible to error (such as along wide continental margins, e.g., Fig. 7). Since such numerical experiments are not subject to the time-constraints of an emergency response, higher resolution grids (requiring longer calculation times) may be employed in order to map the sensitivity of the predictions to the grid spacing used during emergency operations. Finally, assessment of travel times from model-based forecast systems may be used to address the uncertainties of point-source based solutions (e.g., GREENSLADE and TITOV, 2008). The goal of such efforts would be to enable warning centers to calculate and report reasonable error bounds on any estimated time of arrival released to the public.

5. *Conclusions*

1. Simple long-wave predictions of tsunami travel times calculated from a global grid of bathymetry yields approximate results that correlate highly with ~1500 reported travel times from 127 separate events.
2. Large outliers exist on both sides of the expected trend. Observation times that greatly exceed the simple predictions are most likely later arrivals. In cases when predictions greatly exceed observation times we find that either the reports had clerical errors or there were peculiar circumstances with respect to the geometry of the pathways and their depths near a particular station. Because most stations are located next to land, these conditions do occur in enough places to warrant concern.

3. The largest significant causes of uncertainty for predicted travel-times are the inadequate approximation of the tsunami source by the epicenter point source and the poor characterization of shallow bathymetry near stations and some epicenters. Depending on circumstances, the travel-time delays from these errors sources can be significant (i.e., hours).
4. Numerical simulations of hypothetical tsunamis from any point along subduction zones can be performed and used to delineate areas from which the simple travel-time solutions may be inadequate. Likewise, the examination of the variability of travel times near all stations of points of interest can be used to map which regions need special consideration in a warning situation and to guide special processing of bathymetry to ensure the proper representation of key waterways near stations.

Acknowledgments

Diana Greenslade, Gerard Fryer, editor Kenji Satake and an anonymous reviewer made numerous suggestions that lead to improvements in the text. This is SOEST contribution no. 7606.

REFERENCES

ABE, K. (1979), *Size of great earthquakes of 1837–1974 inferred from tsunami data*, J. Geophys. Res. *84*, 1561–1568.

CHRISTENSEN, D. H. and BECK, S. L. (1994), *The rupture process and tectonic implications of the great 1964 Prince William Sound earthquake*, Pure Appl. Geophys. *142*, 29–53.

DUDLEY, W., T*sunami*!, 2nd ed., 380 pp. (Univ. Hawaii Press, Honolulu, 1998).

FRYER, G. J. *et al.* (2004), *Source of the great tsunami of 1 April 1946: A landslide in the upper Aleutian forearc*, Marine Geology *203*(3–4), 201–218.

GEOWARE (2007), *TTT - A tsunami travel-time calculator*, http://www.geoware-online.com

GREENSLADE, D. J. M. and TITOV, V. V. (2008), *A comparison study of two numerical tsunami forecasting systems*, Pure Appl. Geophys. *165*, 1991–2001.

HATORI, T. (1981) *Tsunami magnitude and source area of the Aleutian-Alaska tsunamis*, Bull. Earthquake. Res. Inst., Univ. Tokyo *56*, 97–110.

JOHNSON, J.M. *et al.* (1996) *The 1964 Prince William Sound earthquake: Joint inversion of tsunami and geodetic data*, J. Geophys. Res. *101*(B1):523–532.

JOHNSON, J. M. and SATAKE, K. (1997), *Estimation of seismic moment and slip distribution of the April 1, 1946, Aleutian tsunami earthquake*, J. Geophys. Res. *102*(B6), 11, 765–711,774.

KOWALIK, Z. *et al.* (2005), *Numerical modeling of the global tsunami: Indonesian tsunami of 26 December 2004*, Science of Tsunami Hazards *23*(1), 40–56.

LOPEZ, A. M. and OKAL, E. A. (2006), *A seismological reassessment of the source of the 1946 Aleutian 'tsunami' earthquake*, Geophys. J. Internat. *165*(3), 835–849.

MADER, C.L. (2004), *Numerical Modeling of Water Waves*, 2nd ed., 274 pp. CRC Press, Baton Rouge.

MEI, C. C. (1989), *The Applied Dynamics of Ocean Surface Waves*. (World Scientific, Singapore).

NATIONAL GEOPHYSICAL DATA CENTER (2006), *2-minute gridded global relief data (ETOPO2v2)*, U.S. Department of Commerce, National Oceanic and Atmospheric Administration.

NATIONAL GEOPHYSICAL DATA CENTER (2007) *NOAA/WDC historical tsunami database at NGDC*, edited, http://www.ngdc.noaa.gov/seg/hazard/tsu_db.shtml.

OKAL, E. A. *et al.* (2003), *Near-field survey of the 1946 Aleutian tsunami on Unimak and Sanak Islands*, Bull. Seismol. Soc. Am. *93*(3), 1226–1234.

PACHECO, J. F. and SYKES, L. R. (1992), *Seismic moment catalog of large, shallow earthquakes, 1900–1989*, Bull. Seismol. Soc. Am. *82*, 1306–1349.

PARARAS-CARAYANIS, G. (1967), *A study of the source mechanism of the Alaska earthquake and tsunami of March 27, 1964, I. Water waves*, Pac. Sci. *21*, 301–310.

PLAFKER, G. and SAVAGE, J. C. (1970), *Mechanism of the Chilean Earthquake of May 21 and 22, 1960*, Geol. Soc. Am. Bull. *81*, 1001–1030.

RUFF, L. and KANAMORI, H. (1983), *The rupture process and asperity distribution of three great earthquakes from long-period diffracted P-waves*, Phys. the Earth and Planet. Inter. *31*, 202–230.

SHEPARD, F. P. *et al.* (1950), *The tsunami of April 1, 946*, Bull. Scripps Inst. Oceanogr. Univ. Calif. *5*, 391–528.

SHERBURNE, R. W. *et al. The hypocenter, origin time, and magnitude of the Prince William Sound earthquake of March 28, 1964*. In *The Prince William Sound, Alaska Earthquake of 1964 and Aftershocks* (ed. L. E. Leipold), pp. 49–69 (US Dep. of Comm., Environ. Sci. Serv. Admin., Washington, D.C. 1969).

SMITH, W. H. F. and SANDWELL, D. T. (1994), *Bathymetric prediction from dense satellite altimetry and sparse shipboard bathymetry*, J. Geophys. Res. *99*(B11), 21,803–821,824.

SMITH, W. H. F. and SANDWELL, D. T. (1997), *Global seafloor topography from satellite altimetry and ship depth soundings*, Science *277*(5334), 1956–1962.

WESSEL, P. and SMITH, W. H. F. (1998), *New, improved version of Generic Mapping Tools released*, EOS Trans., AGU, *79* (47), 579.

(Received January 27, 2008, accepted May 10, 2008)
